Journal of Catalysis 433 (2024) 115457

Contents lists available at ScienceDirect

Journal of Catalysis

journal homepage: www.elsevier.com/locate/jcat

Research article

Valorisation of microalga *Chlorella* sp. into furans in the presence of Nb_2O_5 catalysts

Serena Lima [a], Elisa I. García-López [b], Igor Krivtsov [c], Marina Ilkaeva [c,d], Carlos Bornes [d], Luís Mafra [d], Leonarda F. Liotta [e], Silvia Villar-Rodil [f], Juan I. Paredes [f], Giuseppe Marcì [a,*], Francesca Scargiali [a]

[a] Università di Palermo, Dipartimento di Ingegneria, Viale delle Scienze Ed. 6, 90128 Palermo, Italy
[b] Università di Palermo, STEBICEF, Viale delle Scienze Ed. 16, 90128 Palermo, Italy
[c] Department of Chemical and Environmental Engineering, University of Oviedo, Av. Julián Clavería 8, 33006 Oviedo, Spain
[d] CICECO - Aveiro Institute of Materials, Department of Chemistry, University of Aveiro, Campus Universitário de Santiago, 3810-193 Aveiro, Portugal
[e] Institute for the Study of Nanostructured Materials (ISMN)-CNR, via Ugo La Malfa, 153, 90146 Palermo, Italy
[f] Instituto de Ciencia y Tecnología del Carbono (INCAR-CSIC), C/Francisco Pintado Fe 26, 33011 Oviedo, Spain

ARTICLE INFO

Keywords:
Niobium oxide
Heterogeneous catalysis
Biomass valorisation
5-HMF
Algae *Chlorella*

ABSTRACT

Despite the interest in niobia-based catalysts and the importance of biomass valorisation, studies on these catalysts typically utilize model substrates like simple sugars. In this study, a series of niobium oxide-based catalysts was prepared for the application in aqueous phase catalytic conversion of sugars extracted from *Chlorella* sp. microalga into value-added furans. The solid catalysts were firstly characterized by various techniques including X-ray diffraction analysis (XRD), scanning electron microscopy (SEM), thermogravimetric analysis (TGA), Raman and X-ray photoelectron (XPS) spectroscopy as well as low-temperature N_2 physisorption. Moreover, the acidity of the catalysts was assessed by using the temperature-programmed NH_3 desorption (NH_3-TPD), by titration of water suspended catalyst with NaOH solution, and by P-bearing molecular probes loaded catalysts through ^{31}P and ^{1}H solid-state nuclear magnetic resonance (NMR) techniques. Herein, we focused on the catalytic transformation of *Chlorella* sp. and glucose solution as model molecule into furans. The best Nb_2O_5 catalysts for valorizing *Chlorella* sp. into furans exhibited a larger number of Brønsted acid sites, achieving conversion yields to 5-HMF and furfural of ca. 20–22 % with respect to the extracted sugars from algae. The results showed a discernible dependence of the conversion yields to 5-HMF and furfural on catalyst acidity, specific surface area, and the presence of the Brønsted acid sites. Conversely, when using the glucose solution as substrate is concerning, the highest yield to 5-HMF was reached by using a catalyst that showed also the presence of Lewis acid sites. A systematic investigation of the structure–activity relationships in niobium oxide application for aqueous phase dehydration using real biomass substrates to obtain furanic derivatives has not been documented thus far. Therefore, the current research is significant as it demonstrates the feasibility of transforming the carbohydrate content in microalgal biomass into furans by identifying the best catalyst to use.

1. Introduction

Exploration of the alternative and sustainable feedstocks has recently attracted substantial attention because of the shortage, high cost and environmental impact of fossil resources [1]. Biomass, which is available in large amounts and includes all animals, plants, and microorganisms, is an important part of renewable energy [2]. In particular, microalgae are quite attractive as a renewable biomass with a wide range of applications [3]. 5-hydroxymethylfurfural (5-HMF) is one of the top value-added bio-based platform chemicals produced from lignocellulosic biomass or biomass-derived hexose sugars (glucose and fructose) by an acid-catalysed dehydration reaction [4–6]. Furanic derivatives, such as 5-HMF and furfural, obtained from renewable biomass-derived carbohydrates have potential to be sustainable substitutes for petroleum-based building blocks used in production of fine chemicals and plastics such as 2,5-furandicarboxylic acid (FDCA), used

* Corresponding author.
E-mail address: giuseppe.marci@unipa.it (G. Marcì).

https://doi.org/10.1016/j.jcat.2024.115457
Received 2 November 2023; Received in revised form 13 March 2024; Accepted 21 March 2024
Available online 24 March 2024

to produce bio-based polymers [7]. Among other valuable chemicals that can be obtained in the similar processes one can find furfural (2-furaldehyde), an important precursor for various valuable chemical and polymers, synthesized by the xylose (a C5 sugar) dehydration [8] and 2,5-dimethylfuran (DMF), a promising biofuel due to its energy density, 40 % higher than that of ethanol [9].

Acidic catalysts can effectively promote biomass transformation to 5-HMF [4,5]. Many catalytic approaches have been developed for the synthesis of 5-HMF from fructose [5], albeit fructose is an expensive starting material, so its practical application is unrealistic. Alternatively, glucose is an abundant low-cost carbohydrate that could be used for the production of 5-HMF. Nevertheless, the synthesis of 5-HMF is more selective from ketohexoses than from aldohexoses [10], which is probably due to the stable structure of glucose that is also the cause of low yields of its conversion [11] as observed in most of the literature reports [12].

Unlike fructose, which can be dehydrated directly to 5-HMF, glucose conversion requires an additional previous step of isomerization to fructose [5,13–15]. Indeed, the conversion of glucose to 5-HMF is carried out via the isomerization of glucose to fructose in the presence of enzymes or Lewis acid catalytic sites, followed by a dehydration reaction over Brønsted sites [13,14] (see Scheme 1). Consequently, in order to find an economical and environmentally feasible industrial process for the production of 5-HMF, an efficient direct conversion from glucose would be most beneficial. During the conversion of glucose to 5-HMF, several side reactions decrease the selectivity to 5-HMF [4]. These are also indicated in Scheme 1 and include: (i) cross-condensation of glucose with the reaction products; (ii) self-condensation of 5-HMF, leading to the formation of soluble or insoluble oligomers/polymers denominated as humins; (iii) and rehydration of 5-HMF (forming levulinic and formic acids). Different strategies have been attempted to increase the 5-HMF yield, including the use of organic or biphasic solvents as a reaction medium as well as homogeneous or heterogeneous catalysts [4]. The use of organic solvents has been found to enhance the effectiveness of the process. Indeed, the conversion of biomass to 5-HMF has been observed to be lower in aqueous medium than in the presence of organic solvents or biphasic systems, that can improve the selectivity to 5-HMF by suppressing side reactions [16,17]. However, the catalytic system becomes costly and environmentally unfriendly. Besides, glucose is strongly hydrophilic and the glucose coming from the hydrolysis of cellulose or polysaccharides contains water and thus, from this perspective, water is the most desirable, low-cost and eco-friendly solvent for glucose conversion.

The use of a large number of heterogeneous solid acid catalysts, including resins (such as Amberlyst-15), zeolites, niobic acid, zirconia, heteropolyacids, metal phosphates, mesoporous silica and carbon-based catalysts is well documented in the literature for selective synthesis of 5-HMF from glucose under different reaction conditions [4,15]. Among these catalysts Nb_2O_5 stands out as abundant and cheap material with water-tolerant and tunable acid-base properties showing promising performance in sugar conversion reactions [18,19]. Indeed, niobic acid (hydrated niobium pentoxide ($Nb_2O_5 \cdot nH_2O$)) as well as niobium pentoxide (Nb_2O_5), a typically nontoxic solid oxide, exhibit strong redox ability displaying both Lewis acid sites and Brønsted acid sites [20,21], which, as explained above, are needed for the isomerization of glucose to fructose and for the subsequent dehydration of fructose, respectively.

Most of the studies focused on catalytic production of 5-HMF published to date are limited to the use of model monosaccharides as substrates, while for practical purposes the direct conversion of available biomass substrates is indispensable. This, however, is much more challenging because the decomposition of the biomass feedstock strongly depends on the interactions between cellulose, hemicellulose, and lignin. Microalgae are unicellular photosynthetic microorganisms that can fix CO_2 in organic compounds. The use of microalgae as biomass has several advantages as they are more efficient in performing photosynthesis and grow more rapidly than land plants, they can grow in non-arable lands (not competing with edible biomasses) and are used in wastewaters remediation [22]. Furthermore, microalgal biomass may be used in pharmaceutical and cosmetic industries, thanks to its content of high-value bio compounds such as carotenoids, proteins and lipids [23,24].

Although cultivating microalgae with the only intent to extract the carbohydrate fraction may be not economically sustainable, microalgae already employed for wastewater treatment are an ideal source of carbohydrates for finally obtaining furanic derivatives. Microalgal biomass catalytic conversion to furanic products involves its degradation to carbohydrates. However, the microalgal cell wall is a complex structure and many difficulties arise in releasing the carbohydrates from its matrix, in order to make them available for obtaining furanic products. Furtherly, the process implies the hydrolysis of polysaccharides to hexoses and, hence, their isomerization to fructose on Lewis acid sites and its successive dehydration to 5-HMF over Brønsted acid sites [25,26].

Despite the interest in niobia-based catalysts and the importance of biomass valorisation, to the best of our knowledge, a systematic study of the structure–activity relationships in niobium oxide application for aqueous phase dehydration using actual algal biomass substrates to obtain furanic derivatives has not yet been reported. In this work, a set of niobia materials has been prepared and thoroughly characterized. The acidity of the materials was evaluated using temperature-programmed NH_3 desorption (NH_3-TPD) technique, but also applying P-bearing probe molecule-assisted solid-state NMR method enabling acidity assessment of non-thermally treated catalysts allowing for the distinction between Lewis and Brønsted acid sites. The glucose dehydration has been used as model reaction to study its conversion to fructose and subsequently to 5-HMF. Eventually, the microalgal biomass was used as real substrate to obtain 5-HMF and furfural. A previous treatment, in

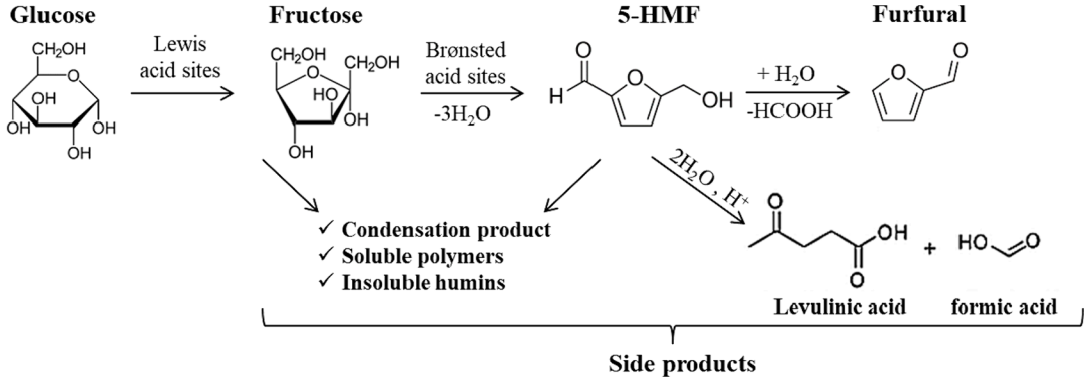

Scheme 1. Reaction scheme for the formation of 5-HMF by the Lewis acid-promoted isomerization of glucose to fructose and Brønsted catalyzed dehydration of the latter. The scheme also shows the formation of the side products of this process.

homogeneous or heterogeneous conditions, was applied to release the carbohydrates from the algae cells and a successive heterogeneous catalytic reaction was carried out in the presence of Nb_2O_5 materials in order to transform the carbohydrates into 5-HMF and furfural. The obtained results suggest that, apart from the optimization of the set-up conditions, the characteristic of the catalysts that mostly affect their activity versus *Chlorella* sp. valorization in terms of conversion yield to furans is their total amount of acid sites. In particular, the best catalysts are those presenting the highest number of Brønsted acid sites. In the presence of these catalysts, conversion yields to 5-HMF and furfural of ca. 20–22 % with respect to the sugars extracted from the algae were obtained.

2. Experimental

2.1. Preparation of the catalysts

A set of niobic acid (Nb_2O_5·n H_2O) catalysts was prepared by using $NbCl_5$ as precursor. 5 g of the precursor was dissolved in 10 mL of ethanol and the pH was increased by adding 200 mL of NH_3 aqueous solution (0.3 mol L^{-1}) to the resulting yellow solution, as reported in a previous study [27]. This procedure leads to a white precipitate of Nb_2O_5·nH_2O, which was washed repeatedly and separated by centrifugation, and eventually dried at 120 °C. It was labelled as Nb_2O_5-T. Alternatively, 5 g of $NbCl_5$ was suspended in 200 mL of water and the resulting precipitate aged under stirring for 3 h and then filtered, washed several times with water until neutral pH and dried overnight at 120 °C. The white precipitate was labelled as Nb_2O_5-E. A third material was synthesized via hydrothermal synthesis. In this case, $NbCl_5$ (0.5 g) was dissolved in 20 mL of water containing nitric acid (0.5 mL HNO_3 65 %), then H_2O_2 (10 mL 30 % v/v) was added to the prepared solution to react with the chloride ions by an oxidation–reduction process, forming Cl_2 and O_2, resulting in a yellow solution (at pH ≈ 0.5) for the presence of the water-soluble niobium peroxo-complex $[Nb(O_2)_4]^{3-}$ species as before reported [28]. The solution was then autoclaved at 120 °C for 24 h and the resulting white solid filtered, washed several times with water and then dried at 100 °C. The obtained solid, named Nb_2O_5-B, was also annealed at 300 or 500 °C for 2 h (heating ramp of 10 °C min^{-1}), resulting in powders labelled as Nb_2O_5-B-300 and Nb_2O_5-B-500. Two commercial solids were also tested for the sake of comparison, i.e. niobic acid (commercial name HY-340) kindly provided by Companhia Brasileira de Metalurgia e Mineração (CBMM) and Nb_2O_5 Sigma Aldrich (labelled in the following as Nb_2O_5-SA).

All other chemicals were purchased from Sigma Aldrich with assay of 99.99 % and used as received without any further purification. Water used throughout the experiments was purified by means of a Milli-Q system.

2.2. Materials characterisation

Bulk and surface characterizations were carried out in order to investigate the structural, textural and physicochemical properties of the powders. Powder XRD patterns were registered in an X'pert PAN-analytical diffractometer (step size of 0.0167° and scan speed of 1.28° min^{-1}), using a Ni-filtered Cu-Kα radiation source and PixCel1D (tm) detector.

The specific surface areas (SSA), pore volume and pore size of the materials were determined from N_2 adsorption–desorption isotherms using a Micromeritics ASAP2020 system. Before analysis, the samples were degassed under vacuum at 100 °C for 12 h, then the measurement was performed at liquid nitrogen temperature (-196 °C). The low pre-treatment temperature was applied, in order not to modify the properties of non-calcined materials. The Brunauer-Emmett–Teller (BET) method was used to calculate the SSA. Mettler Toledo TGA/SDTA851 was used to investigate the thermal decomposition of the Nb_2O_5 samples under an O_2 flow of 50 mL min^{-1} in the temperature range 25 to 1000 °C with a heating rate of 10 °C min^{-1}. Scanning electron microscopy (SEM) was performed using a FEI Quanta 200 ESEM microscope, operating at 20 kV on specimens upon which a thin layer of gold had been evaporated.

Transmission Electron Microscopy (TEM) was performed using a Hitachi HD-2700 apparatus at an acceleration potential of 200 kV.

Raman spectra were recorded on powdered samples packed into sample cups. Spectra were registered by using a Renishaw in-via Raman spectrometer equipped with an integrated microscope and with a charged-coupled device (CCD)camera. A He/Ne laser operating at 632.8 nm was used as the exciting source. The power of the laser used was 15 % of the maximum value that was around 300 mW. Three different measures on the same sample were carried out in different positions on the specimen to confirm the homogeneity and reproducibility of the measure. X-ray photoemission spectroscopy (XPS) analysis of the powdered catalysts was performed on a SPECS spectrometer equipped with a Phoibos 100 hemispherical electron energy analyser. The spectra were acquired at pressure below 10^{-7} Pa using a monochromatic Al K_α X-ray source operated at a voltage of 14.00 KV and a power of 175 W. The photo-excited electrons were analysed in constant pass energy mode, using pass energy of 50 and 10 eV for the survey and the high-resolution core level spectra, respectively. The spectra were recorded at a take-off angle of 90°. As the Nb_2O_5 catalysts are electrical insulators, a net positive charge built up on their surface upon photoemission of electrons, which was compensated with an electron flood gun.

The acidic properties of the prepared catalysts in terms of Brønsted and Lewis acid sites were studied by NH_3-TPD that were performed using a Micromeritics Autochem 2950 instrument equipped with an ultraviolet gas analyser (ABB, Limas 11). Before starting the ammonia adsorption experiment, the sample was pre-treated in He flow at 200 °C for 30 min. After cooling to room temperature, a stream of 5 % NH_3/He (30 mL min^{-1}) was flowed over the sample for 1 h. To remove physically adsorbed ammonia, the sample was purged in flowing He (100 mL min^{-1}) at 100 °C for 1 h, then, cooled down to room temperature. Ammonia desorption was monitored with the above-mentioned ABB, UV gas analyser (the concentration of ammonia (ppm) was registered in the flow with the step of one second), under He flow (30 mL min^{-1}) heating up to 600 °C (rate of 10 °C min^{-1}). At 600 °C the ammonia was totally desorbed and the acquisition of data was stopped. Before the gas detection system, a cold trap was used to condense any water desorbed from the sample. The ammonia concentration profiles, ppm of NH_3 desorbed g^{-1} s^{-1} under He flow were plotted versus time and temperature and the total amount of desorbed NH_3 [mmol NH_3 g^{-1}] was then calculated by the integration of the curves.

The total acidic strength was determined also by titration with 0.01 M NaOH (aq) as previously reported for acidic solids [27]. In a typical experiment, 0.1 g of solid was added to 25 mL of deionized water. The resulting suspension was allowed to equilibrate under stirring for 24 h and thereafter it was titrated by dropwise addition of 0.01 M NaOH solution using phenolphthalein as pH indicator.

Further investigations on the acidity of the samples were carried out by magic-angle spinning (MAS) solid-state NMR (ssNMR). Trimethylphosphine oxide (TMPO) adsorption on the catalytic material was performed to obtain ^{31}P and ^{1}H ssNMR spectra. TMPO-loaded samples were prepared using modified procedure reported in the literature [29,30]. In this work, 40 mg of TMPO was dissolved in 5 mL of dry dichloromethane in a nitrogen-filled glove box under a constant N_2 flow followed by the addition of 60 mg of the corresponding niobium oxide sample that had not undergone additional dehydration. After stirring for 4 h under N_2, the solvent was evaporated under vacuum and the sample was left for drying under vacuum for at least 14 h. Finally, the sample was packed in a 4 mm zirconia rotor in a N_2 glove box prior to ssNMR analysis. SSNMR is widely used to determine nature and strength of acid sites in oxides where TMPO is used as P-bearing probe molecule [31–33]. ^{1}H MAS ssNMR spectra of the niobium oxide samples were acquired on a Bruker Avance III 400 and 700 spectrometers operating at B_0 field of 9.4 and

16.4 T corresponding to ^{1}H Larmor frequencies of 400.1 and 700.1 MHz, respectively. ^{31}P MAS and cross-polarization (CPMAS) ssNMR spectra were acquired on a Bruker Avance III 400 spectrometer corresponding to ^{31}P Larmor frequency of 162 MHz. Experiments were performed on a double- and triple resonance 4 mm Bruker MAS probe, except for some ^{1}H MAS measurements, in which a double resonance 1.9 mm Bruker MAS probe was used. Samples were packed into 1.9 or 4 mm zirconia rotors using Vespel and Kel-F caps, respectively. Chemical shifts were quoted in ppm using the following secondary references: solid adamantane (1.85 ppm) and solid $Na_4P_2O_7$ (-2.09 ppm for the most shielded resonance) for ^{1}H and ^{31}P, respectively. In case of 1.9 mm probe, ^{1}H single-pulse experiments were acquired at a spinning rate of 40 kHz using a 90° pulse of 2.2 μs corresponding to a radiofrequency (rf) field strength of 113 kHz. When using 4 mm double-resonance/triple-resonance probes (the results for the triple-resonance probe are indicated in parenthesis), ^{1}H-decoupled ^{31}P MAS NMR spectra were acquired at a spinning rate of 15 kHz using a pulse length of 3.25 (2.97) μs corresponding to a rf field strength of 77 (84) kHz, employing a 60° (40°) flip angle. In all cases, a recycle delay (RD) of 15 s was used. Two-dimensional (2D) ^{1}H-^{31}P heteronuclear correlation (HETCOR) NMR spectra were acquired using a ^{1}H 2.75 (3.25) μs pulse length (90° flip angle) corresponding to a rf of 91 (77) kHz. The cross-polarization step was performed using a contact time of 5000 (8000) μs with a 70–100 % Ramp shape on the ^{1}H channel and a square shaped pulse of 49 (37) kHz on the ^{31}P channel, a RD of 1.5 s and a spinning rate of 15 kHz. A SPINAL-64 decoupling scheme was used with pulse length of 6.0 (5.5) μs at a rf field strength of 79 (82) kHz. 74 (1 3 4) t1 points with at least 1 k scans each were recorded along the indirect dimension.

The concentrations of Nb and P elements present for all TMPO-loaded niobium oxide samples were determined by inductively coupled plasma - optical emission spectrometry (ICP-OES).

2.3. Heterogeneous catalytic activity: Hydrothermal conversion of glucose

Typically, 24 mL of a 2.3 mM glucose aqueous solution (414 ppm) and 0.024 g of catalyst were introduced in the autoclave reactor. A stainless-steel autoclave hydrothermal reactor (Tefic Biotech Co. Limited, Xian, China) with a 50 mL PTFE chamber was used. The autoclave was introduced into a thermostatic preheated synthetic oil bath placed on a hot magnetic stirrer. Once the oil temperature reached the established value (180 °C), the reactor was immersed in the bath and the reaction time started. The reactor was maintained under stirring for 1 h. Then, it was quickly cooled down to room temperature in a water bath. After that, the suspension was filtered using 0.2 μm membranes (CA, Millipore) to separate the catalyst and the solution aliquot was analysed. The compounds in the reaction mixture were identified and quantified by means of a Thermo Scientific Dionex Ultimate 3000 HPLC equipped with a Diode Array and a Refractive Index detectors. A REZEK ROA Organic acid H^+ Phenomenex column was used with an aqueous 2.5 mM H_2SO_4 solution as eluent with a flow rate of 0.6 mL min^{-1}. Retention times and UV spectra of the compounds were compared with those of standards purchased from Sigma-Aldrich with a purity >99 %. Commercial standards of 5-HMF, furfural, glucose and fructose were used in order to identify and confirm their presence in the reacting medium and to build the calibration curves for the calculation of their concentrations in reaction mixtures.

The performance of Nb_2O_5 solid acid catalysts in the glucose isomerization/dehydration reactions was evaluated in terms of conversion (X) of the hexose, selectivity (S) to fructose and 5-HMF and yield (Y) of 5-HMF, which were defined as follows:

$$X = \frac{[glucose]_i - [glucose]_f}{[glucose]_i} \bullet 100 \quad (1)$$

$$S_{fructose} = \frac{[fructose]_f}{[glucose]_i - [glucose]_f} \bullet 100 \quad (2)$$

$$S_{HMF} = \frac{[HMF]_f}{[glucose]_i - [glucose]_f} \bullet 100 \quad (3)$$

$$Y_{HMF} = \frac{[HMF]_f}{[glucose]_i} \bullet 100 \quad (4)$$

where $[glucose]_i$ and $[glucose]_f$ are the initial and the final molar concentrations of glucose, respectively, and $[fructose]_f$ and $[HMF]_f$ are the molar concentrations of fructose and 5-HMF, respectively, at the end of the experiment.

2.4. Algal growth and analysis of the carbohydrate content of the biomass

Microalgae *Chlorella sp*. Pozzillo was previously isolated from Sicilian littoral [22]. The strain was kept in liquid medium where a commercial fertilizer (Spray-feed, Pavoni) diluted in water was employed at the concentration of 3 gL^{-1}. A pre-culture of the microalgae was set up by inoculating 10 mL of sample from a culture flask in 100 mL of fresh medium. When cells were in late exponential phase (after about 10 cultivation days), 10 mL of the cell suspension was used to inoculate the medium containing cultivation flask (growth medium cultivations) or sewage (first and second cultivations). The algae were cultivated for 15 days under a photon flux density of about 200 μmol m^{-2} s^{-1} in 1 L Erlenmeyer flasks placed in an oscillating incubator (Corning Lse) at 100 rpm. Light intensity (in the range of wavelengths 400–700 nm) was measured with a Delta Ohm-HD 9021 quantometer equipped with a Photosynthetic Active Radiation (PAR-) probe (Delta Ohm LP 9021 PAR). After the batch cultivation, the biomass was harvested by centrifugation and frozen in liquid nitrogen and freeze-dried for 24 h in a bench lyophiliser (FreeZone 2.5 L, LABCONCO, US). The biomass obtained from several cultivations was collected together and homogenised.

For the quantification of total carbohydrates in the algae the National Renewable Energy Laboratory (NREL) protocol was used [34]. In particular, 20 mg of freeze-dried (lyophilized) biomass were weighted in a glass tube and 250 μL of H_2SO_4 72 % were added. The mixture was vortexed and kept for 1 h at 30 °C. After that, 7 mL of water were added to adjust the H_2SO_4 concentration to 4 % and the glass tube was tightly closed and placed in an autoclave for 1 h at 121 °C. After that, the suspension was filtered through 0.2 μm membranes (CA, Millipore) and the obtained sugars (glucose and fructose) were analysed by means of the same HPLC apparatus described earlier in section 2.3.

2.5. Heterogeneous catalytic activity: Hydrothermal conversion of *Chlorella sp.*

An amount of 40 mg of the lyophilized *Chlorella* sp. was dispersed in 24 mL of water and the suspension was placed in the same autoclave reactor that was used for the glucose transformation. The catalytic experiments were performed both in homogeneous and heterogeneous regimes, by employing either HCl (0.7, 2, and 7.0 % wt) or Nb_2O_5 (1 g L^{-1}). Moreover, selected experiments were carried out in presence of SiO_2 beads (10 g L^{-1}, Riedel-de Haen; 0.2–0.5 mm size). Reaction conditions such as time and temperature, along with catalysts/biomass mass ratio were varied, in order to assess their effect on the reaction outcome and optimise the performance of the system.

Further experiments were carried out in two stages. The first aimed at the extraction of sugars from the biomass and the second one at the transformation of the sugars obtained into furans. In the first step, 40 mg of biomass in 24 mL of water and 240 mg of SiO_2 beads were placed in the autoclave and kept for 2 h at 140 or 180 °C. For selected runs, acetic acid was added to reach pH 4. The second step was performed in the presence of Nb_2O_5 at 180 °C. The experiments were carried out during different reaction times. In all cases, the reactor was cooled down at the end of the reaction and the suspension filtered and analysed by HPLC as

described in section 2.3. The course of the reaction, both in homogeneous and heterogeneous conditions, was evaluated in terms of total yield (Y_F) to furans (5-HMF as majority and furfural as minority observed species) from the sugars contained in the algae:

$$Y_F = \frac{[HMF]_f + [furfural]_f}{[\text{total sugar in biomass}]} \bullet 100 \quad (5)$$

where ($[HMF]_f$ and $[furfural]_f$ are the concentrations of the products measured in solution after the reaction, and [total sugar in biomass] is the total concentration of sugars from the algae matrix quantified by the NREL protocol.

3. Results and discussion

3.1. Solid catalyst characterization

In order to investigate the crystalline structure of the prepared materials, XRD patterns were registered. All as-prepared niobic acid samples and the commercial HY-340 niobium oxide show typical patterns of amorphous materials as demonstrated in Fig. 1. The calcination of the hydrothermally synthesized Nb_2O_5 at 500 °C (Nb_2O_5-B-500) yields a crystalline niobium pentoxide, whose diffraction pattern coincides with that of the commercial Nb_2O_5-SA and corresponds to the low-temperature orthorhombic Nb_2O_5 crystal phase (#1840 ICSD). Unlike the commercial niobium oxide (65 nm), the home-prepared Nb_2O_5-B-500 has a much smaller crystallite size (17 nm) (Table 1).

The preparation techniques used in this work to obtain niobium oxides or niobic acid greatly affect the textural properties of the resultant materials. The sample of niobium oxide prepared by precipitation with ammonia (Nb_2O_5-T) shows the lowest surface area and meso- and micro-pore volumes among all home-prepared materials with values of 85 $m^2\ g^{-1}$ and 0.06 $cm^3\ g^{-1}$, respectively (Fig. 2A, Table 1). In contrast, the sample Nb_2O_5-E (Fig. 2A) follows an isotherm of type I(b), typical for microporous solids [35]. In addition, this sample possesses high specific surface area of 323 $m^2\ g^{-1}$ (Table 1). Upon calcination of the as-prepared niobic acid, the Nb_2O_5-B sample series reveal clear evolution of mesoporosity (Fig. 2C). The isotherm of hydrothermally prepared Nb_2O_5-B most likely can be assigned to a mixed I(b) and IV(a) type with barely distinguishable hysteresis loop (Fig. 2B). The presence of micropores in this material is accompanied by mesopores of small size (3 nm) accounting for their total pore volume of 0.16 $cm^3\ g^{-1}$ (Table 1). Although the thermal treatment of this material (up to 300 °C) is not sufficient to convert it into a nonporous crystalline oxide, it greatly affects its textural properties. The isotherm of hydrothermally prepared niobia samples subsequently calcined at 300 °C (Nb_2O_5-B-300) assumes the shape more typical of mesoporous solids (type IV(a) with an H2(a) type hysteresis) (Fig. 2B). As the result, this sample exhibited narrowly distributed mesopores (Fig. 2C). Further thermal treatment of Nb_2O_5-B at higher temperature (500 °C) leads to crystalline oxide phase (adsorption isotherm of type II) with low SSA of 50 $m^2\ g^{-1}$ and reduced pore volume (Table 1). The mesopores, whose presence is indicated by the hysteresis loop at high P/P_0, are large and have a broad size distribution, most likely attributed to the interparticle porosity (Fig. 2C, Table 1).

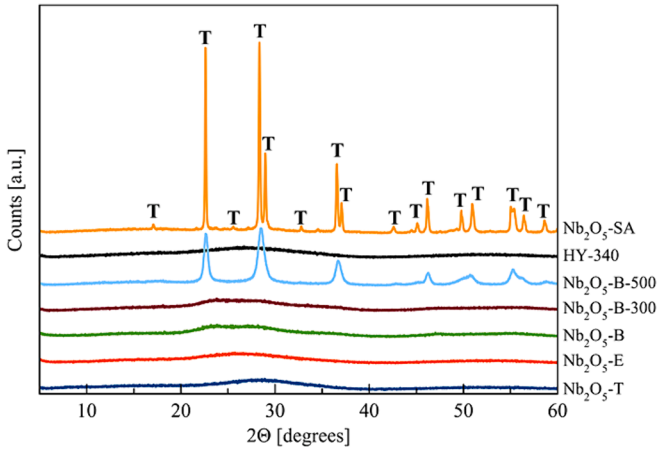

Fig. 1. Powder XRD patterns of the synthesized and commercial Nb_2O_5 catalysts. T - stands for the XRD reflections corresponding to the low-temperature orthorhombic Nb_2O_5 crystal phase (#1840 ICSD).

Thermogravimetric analysis of the commercial Nb_2O_5-SA sample shows almost complete absence of mass loss up to 1000 °C, which agrees with its highly crystalline nature (Figs. 1 and 3). The other commercial material, the amorphous HY-340, shows a significant mass loss of about 15 % in the low-temperature range up to 300 °C that is most likely attributed to release of water (Fig. 3). All the as-prepared samples Nb_2O_5-T, Nb_2O_5-E, Nb_2O_5-B also show the loss of water upon heating up to 300 °C accounting for 22 %, 26 % and 23 % of mass loss, respectively, indicating the hydrated state of these oxides. The calcination of the Nb_2O_5-B material gradually eliminates the bonded water and turns this amorphous oxide into a crystalline solid with almost negligible mass loss of about 3 % for Nb_2O_5-B-500 (Fig. 3).

The various catalysts tested in this work show very different morphologies (Fig. 4). As far as the home prepared samples are concerned, the catalyst Nb_2O_5-T consists of agglomerates of particles with dimensions less than 8 nm. For the catalyst Nb_2O_5-E, it is not possible to identify the size of the particles constituting the agglomerates, as they appear fused together. Both the non-calcined and calcined (300 and 500 °C) Nb_2O_5-B materials, did not show significant differences in their morphologies, as depicted in Fig. 4. In all three cases, the catalysts appear to consist of agglomerates of particles ranging from ca. 25 to 30 nm in particle size. The only difference is that the delineation of the agglomerate shapes is more defined as the calcination temperature increases, reaching dimensions up to about 600 nm. In contrast, the commercial sample (Nb_2O_5-SA) seems to consist of very well-defined particles (crystals) having broad size distribution. For example, the particle sizes that can be seen in Fig. 4 range from ca. 28 to ca. 140 nm. On the other hand, the HY-340 sample appears to form nanosized agglomerates that are not well-defined, whose dimensions vary between 11 and 16 nm.

In order to confirm or not the results on the crystallite and/or particles size and the porosity of the niobic acid samples found through the XRD and adsorption/desorption isotherms of N_2 studies, respectively, a TEM investigation was carried out on some selected samples. It was decided to perform this investigation on Nb_2O_5-B, Nb_2O_5-B-300 and Nb_2O_5-B-500 because in this way was also possible to study the evolution of niobic acid samples by the thermal treatment at two different temperatures.

TEM images of the selected samples are presented in Fig. 5. The non-calcined niobic acid material, Nb_2O_5-B, is composed of filamentous aggregates of smaller particles of amorphous nature, according to the XRD data (Fig. 5(A, D)). Upon calcination the material's morphology suffers certain transformations. At first, after being treated at 300 °C, the Nb_2O_5 sample loses the filament-like appearance and the presence of separate small particles becomes evident (Fig. 5(B, E)). Finally, after the calcination at 500 °C (Fig. 5(C, F)) the formation of Nb_2O_5 crystallites in the range of 10–24 nm is observed corroborating the results obtained from the XRD analysis (Table 1). The TEM observations are in accord with the XRD and SSA analysis results showing the oxide crystallization and the particles growth that is accompanied by the loss of SSA. Additionally, it is revealed that the porosity detected by the N_2 adsorption experiments (Fig. 2, Table 1) most likely is due to the interparticle voids.

Raman spectroscopy was employed to further investigate the structural features of the catalysts as it offers high sensitivity for phase analysis. The Raman spectra (Fig. 6) of all amorphous niobic oxides and niobic acids (Nb_2O_5-T, Nb_2O_5-E, Nb_2O_5-B, Nb_2O_5-B-300 and HY-340)

Table 1
Textural properties of the prepared and commercial catalysts.

Catalyst	Mean crystallite size [nm][a]	SSA [m^2g^{-1}]	Total pore volume [cm^3g^{-1}][b]	Micropore volume [cm^3g^{-1}][c]	Mesopore volume [cm^3g^{-1}][d]	Mean mesopore size [nm][e]
Nb_2O_5-T	–	85	0.06	0.04	0.02	3.6
Nb_2O_5-E	–	323	0.17	0.14	0.03	3.0
Nb_2O_5-B	–	320	0.28	0.12	0.16	3.0
Nb_2O_5-B-300	–	206	0.29	0.07	0.22	3.7
Nb_2O_5-B-500	17	50	0.19	0.02	0.17	9.6
Nb_2O_5-SA	65	3	0.01	–	–	–
HY-340	–	107	0.13	0.04	0.09	4.4

[a] mean crystallite size calculated by Scherrer equation using (0 0 1) reflection of T-Nb_2O_5 phase.
[b] calculated from the adsorbed N_2 amount at $P/P_0 = 0.99$.
[c] calculated using Dubinin-Radushkevich model.
[d] mesopore volume calculated as V_{total}-V_{micro}.
[e] average mesopore size calculated from the desorption branch using BJH approach.

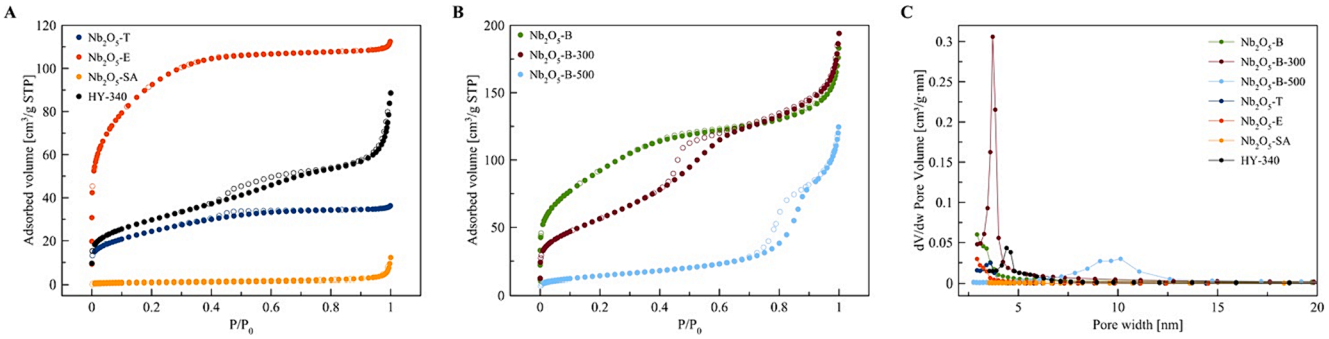

Fig. 2. Adsorption-desorption isotherms of N_2 at 77 K registered for the niobium oxide samples (A-B) with BJH pore size distribution (C). Filled and open symbols represent the adsorption and the desorption branches, respectively.

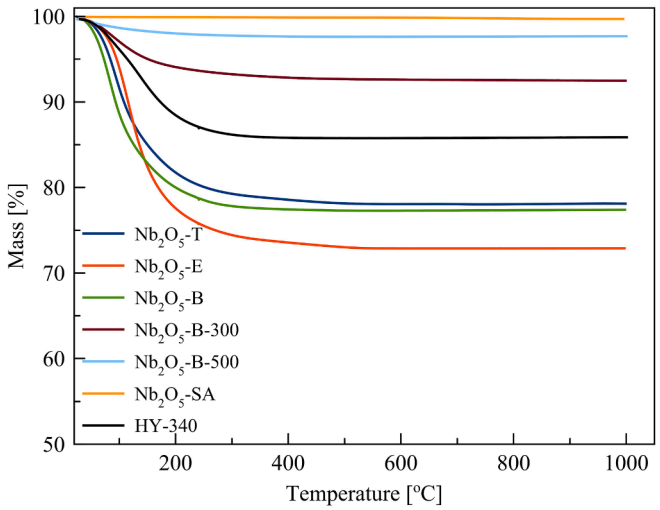

Fig. 3. Thermogravimetric analysis of the synthesized and commercial Nb_2O_5 samples. Measurements were carried out under an O_2 flow of 50 mL min^{-1} in the temperature range 25 to 1000 °C with a heating rate of 10 °C min^{-1}.

show a broad band centred at about 650 – 670 cm^{-1}. This vibration band is assigned to the symmetric stretching mode of distorted niobia polyhedra and reflects the distribution of NbO_6, NbO_7 and NbO_8, in amorphous Nb_2O_5 oxide or niobic acid. In these structures, each Nb atom is surrounded by six or seven oxygens, forming distorted octahedra or bipyramids, which are joined by edge or corner sharing [36–39]. The heat treatment of the amorphous niobia increases the Nb–O bond order, thus resulting in the blue-shift of this band (to higher wavenumbers up to 690–700 cm^{-1} [40]). The vibrational bands around 700 cm^{-1} reveal the presence of the Nb_2O_5 orthorhombic T-phase in the calcined materials (Nb_2O_5-B-500 and Nb_2O_5-SA) thus agreeing with the results obtained by the XRD analysis. A group of weak and broad bands in the low-wavenumber region (200–300 cm^{-1}) is assigned to the bending vibrational modes of the Nb–O–Nb linkages in the T-Nb_2O_5 structure [41].

XPS analysis (Fig. 7) revealed that all the materials showed Nb 3d bands consistent with Nb state in crystalline Nb_2O_5 (maxima of the Nb $3d_{5/2}$ spin–orbit components at binding energy of 207.5 eV [42]). The full-width at half-height for Nb $3d_{5/2}$ peaks is also equivalent for all materials within experimental error (1.0–1.1 eV) except for the case of Nb_2O_5-B, that shows a wider band (1.4 eV), suggesting a chemical environment around Nb atoms at the surface that is similar in all the catalysts, although slightly more heterogeneous for Nb_2O_5-B.

3.1.1. *Acidic properties*

The acidic properties of the thermally treated Nb_2O_5-B catalysts (i.e., Nb_2O_5-B-300 and Nb_2O_5-B-500 materials) were evaluated by NH_3-TPD experiments carried out from room temperature up to 600 °C under helium flow. According to the literature [43] NH_3 desorption in the range 200–250 °C corresponds to weak acid sites, between 250 and 350 °C to medium acid site strengths and above 350 °C assigned to strong acid sites. Fig. 8 displays the process of desorption of NH_3 from the catalyst surface as a function of the temperature. Table 2 lists the acidity values derived from the NH_3-TPD study in terms of the total amount of desorbed NH_3 [mmol $NH_3{\cdot}g^{-1}$]. The NH_3-TPD profile of Nb_2O_5-B-500 is characterized by a very broad peak covering almost the entire window of temperature, 200–500 °C, with an area corresponding to 1.38 mmol $NH_3{\cdot}g^{-1}$. The peak of NH_3 desorption centred at around 330 °C is attributed to weak and medium acid sites. Conversely, strong acid sites were mainly detected in the Nb_2O_5-B sample calcined at 300 °C, Nb_2O_5-B-300, by the presence of a strong desorption peak at 395 °C. The total acidity of this sample accounts for 1.71 mmol $NH_3{\cdot}g^{-1}$ being the highest amongst the studied materials. Moreover, some weak

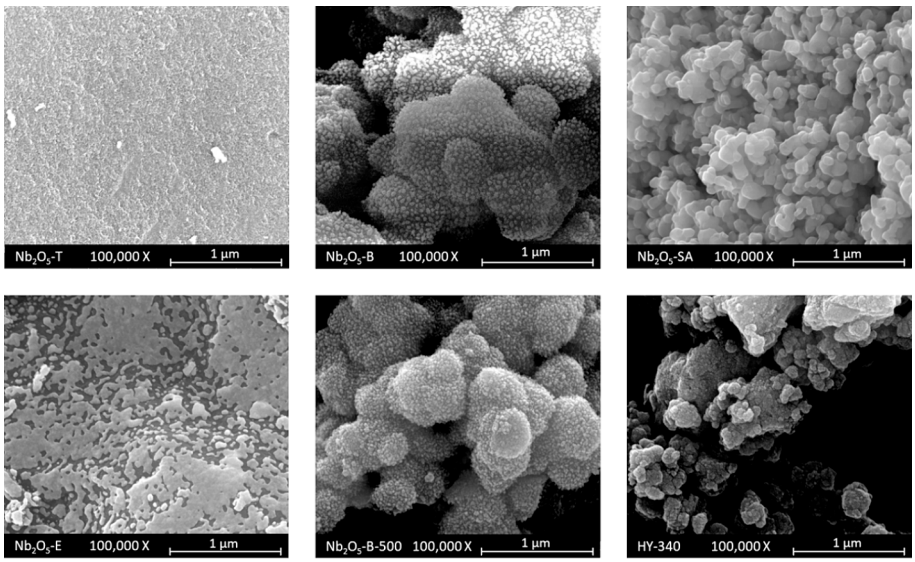

Fig. 4. SEM micrographs of the catalysts. The name of the catalyst is depicted in each picture.

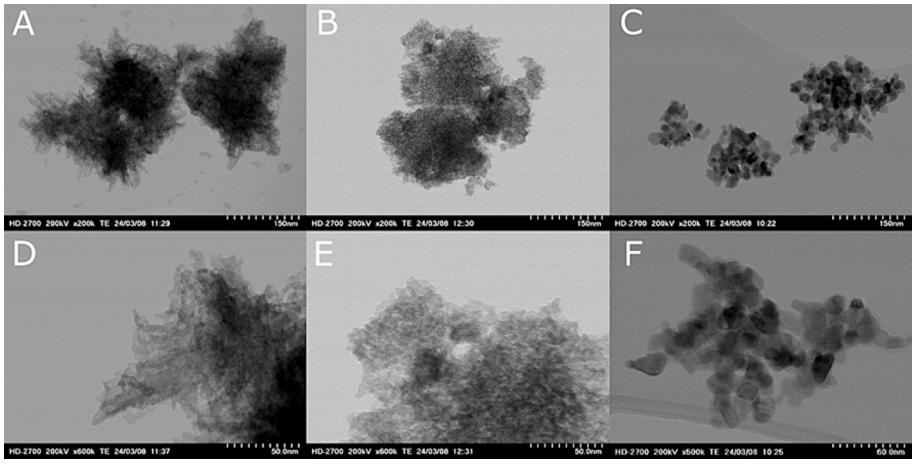

Fig. 5. TEM images of the prepared samples taken at different magnifications: Nb_2O_5-B (A, D), Nb_2O_5-B-300 (B, E) and Nb_2O_5-B-500 (C, F).

and medium acid sites also contribute to the overall acidity as can be concluded from the shoulder presented between 200 and 300 °C.

Nb_2O_5-T displays a similar NH_3 desorption profile as that of Nb_2O_5-B-300. The maximum of ammonia desorption for Nb_2O_5-T is at around 365 °C and the concentration of total acid sites for such sample is 1.59 mmol $NH_3 \cdot g^{-1}$. Moreover, the TPD curve of Nb_2O_5-T at 200–300 °C depicts a more pronounced shoulder than for Nb_2O_5-B-300, indicating that for Nb_2O_5-T, the weak and medium acid sites contribute to the overall acidity at higher extent. Regarding the commercial HY-340 sample, it can be observed that the temperature peak of the NH_3 desorption curve is approximately at 345 °C and the concentration of total acid sites resulted of 1.50 mmol $NH_3 \cdot g^{-1}$. However, this peak is much narrower compared to that of the previous two samples. This fact suggests a tighter distribution of acidic sites in the HY-340 compared to those present in the home-prepared samples.

Finally, very poor acidity was detected for Nb_2O_5-SA as observed by the very weak and broad desorption curve, corresponding to only 0.03 mmol $NH_3 \cdot g^{-1}$.

Unfortunately, the NH_3-TPD measurements for samples Nb_2O_5-B and Nb_2O_5-E were not reproducible and then they are not reported in Fig. 8. This lack of reproducibility is likely due to the high acidity observed with the titration method (see Table 2) and the significant amount of water released during heating (see TGA).

For the sake of comparison, acidity strength was also determined by titration of the powders suspended in water with NaOH (0.01 M) solution. The concentration of acid sites of the catalysts are summarized in Table 2. Such measurements evidenced the higher acidity of the non-calcined Nb_2O_5 samples with respect to both, the one calcined at 500 °C and the commercial Nb_2O_5-SA powder, that resulted the least acidic material.

The results obtained by the two above-mentioned techniques are in good agreement, confirming the higher content of acid sites in the Nb_2O_5-T, Nb_2O_5-B-300 and HY-340 compared to Nb_2O_5-B-500 and Nb_2O_5-SA. The slightly higher acidity, measured by NH_3-TPD, for the Nb_2O_5-B-300 compared to the Nb_2O_5-T sample can be attributed to the presence of Lewis acid sites not detectable by NaOH titration.

Atomic-level insight into the distribution of Lewis and Brønsted acid sites in the niobia materials can be obtained by solid-state NMR investigation as discussed ahead.

The ^1H spectra of assorted bare Nb_2O_5 samples studied in this work are reported in Fig. 9(A). The resonance near 5.5 ppm is ascribed to the bridging OH-groups and residual adsorbed water [44]. A decrease of this resonance can be noticed with the increase of the treatment temperature. Not surprisingly, this peak is barely distinguishable for the commercial Nb_2O_5-SA, which is in the agreement with XRD data thus confirming its high crystallinity degree (Fig. 1) and, consequently, low

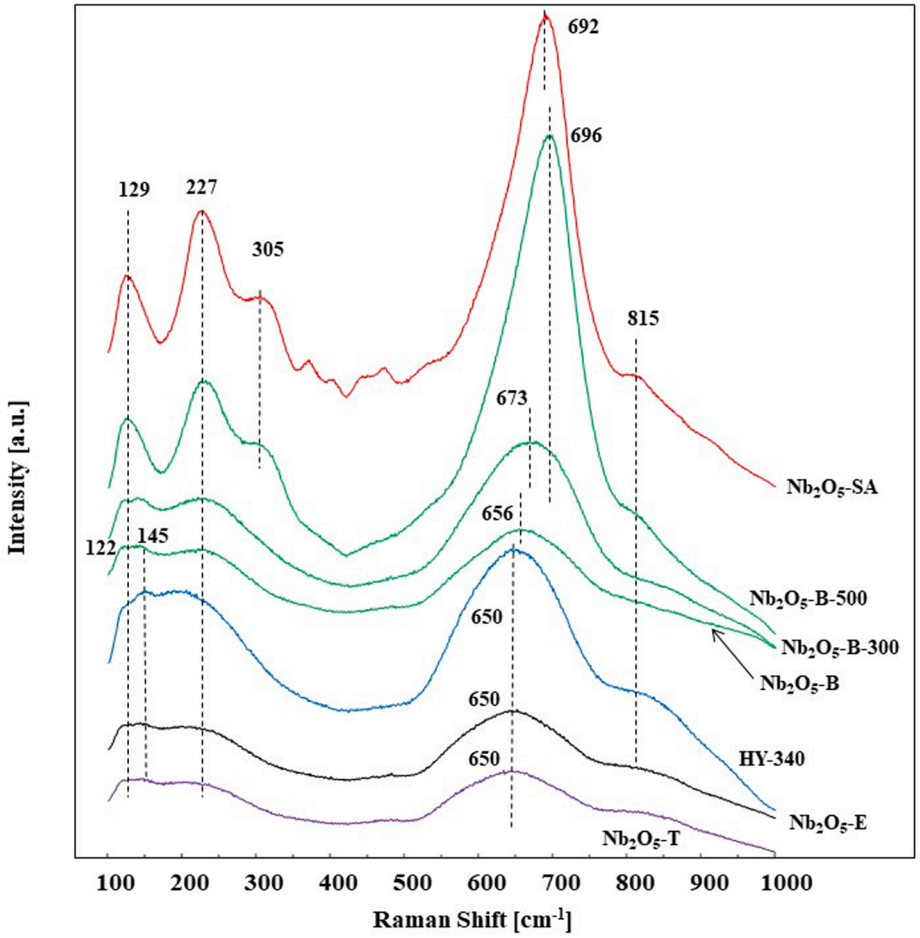

Fig. 6. Raman spectra of the synthesized and commercial catalysts.

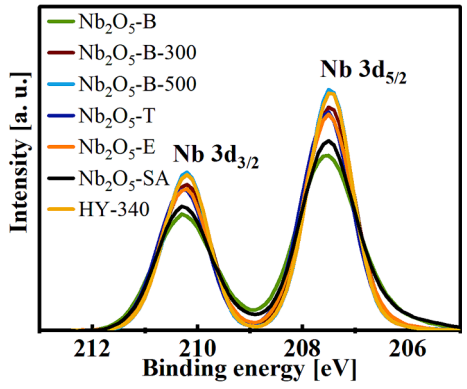

Fig. 7. Normalised, background-subtracted Nb 3d XPS core level spectra of the catalysts. The components of the spin–orbit doublet have been labelled for clarity.

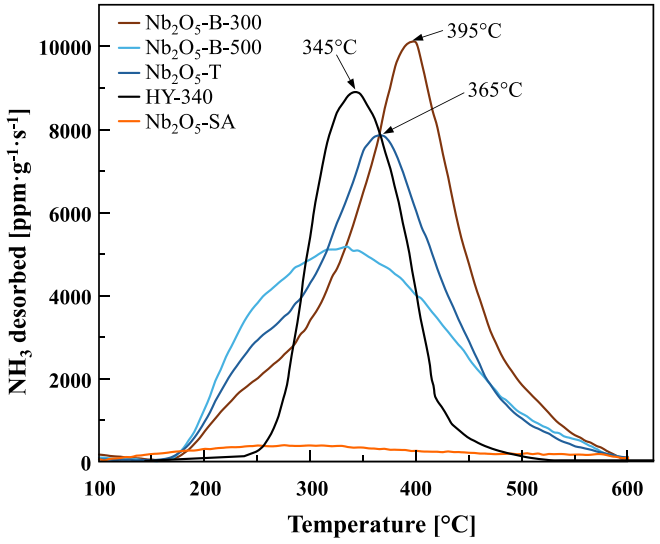

Fig. 8. NH_3-TPD curves of the prepared catalysts registered as a function of the temperature.

number of OH-groups and coordinated water molecules should be expected. This fact is also confirmed by the TGA study (Fig. 3), which indicates a negligible mass loss up to 1000 °C in the case of the latter sample. ^{1}H resonances appearing between 0.5 and 1.5 ppm correspond to the terminal OH-groups [44,45]. Interestingly, the most resolved peaks in this area arise from the Nb_2O_5-B and Nb_2O_5-B-300 samples, (Fig. 9(A) inset) although the overall intensities are low comparing to the 5.5 ppm peak. Fig. 9(B) shows the ^{1}H spectra of the prepared samples loaded with the TMPO probe molecule where new resonances appear. The most intense peak at 1.5 ppm is attributed to the protons of the TMPO methyl groups.

Chemical nature of active sites in the prepared oxides were assessed by ^{31}P (CP)MAS using TMPO as a local probe molecule for acid sites. ^{1}H-decoupled ^{31}P MAS and ^{31}P CPMAS NMR spectra of the synthesised catalysts are shown in Fig. 9. The ^{31}P resonances at 39 and 42 ppm are

Table 2
Acidic properties of prepared catalysts as determined by TPD-NH_3 and by NaOH (0.01 M) titration.

Catalyst	Total acid sites [mmol $NH_3 \cdot g^{-1}$]	Acid capacities by NaOH titration [mmol $H^+ \cdot g^{-1}$]
Nb_2O_5-T	1.59	0.750
Nb_2O_5-E	–	1.69
Nb_2O_5-B	–	1.92
Nb_2O_5-B-300	1.71	0.635
Nb_2O_5-B-500	1.38	0.160
Nb_2O_5-SA	0.03	0.156
HY-340	1.50	0.694

attributed to crystalline TMPO (non-adsorbed TMPO) reflecting the fact that an excess of TMPO was introduced into the system, and thus implying that all acid sites in the niobium oxide sample were saturated [46]. It is known that when reacting with the Brønsted acid sites of oxides, TMPO converts into its protonated state ($TMPOH^+$) exhibiting ^{31}P resonances at higher chemical shifts, typically above 60 ppm. A broad resonance observed for the Nb_2O_5-B and Nb_2O_5-B-300 near 60–65 ppm is usually assigned to the presence of Brønsted acid sites of medium strength as observed in other works on niobium oxides systems [29,30]. Whereas ^{31}P MAS spectra of Nb_2O_5-B-500 reveals significantly reduced intensity in this ppm range most likely due to the dehydration occurring during the calcination at high temperature resulting in the loss of SSA and acid sites (Fig. 10(A)). ^{31}P CPMAS spectrum of Nb_2O_5-B-500, unlike the cases of Nb_2O_5-B and Nb_2O_5-B-300, revealed signals of low intensity near 60 ppm (Fig. 10(B)) suggesting that there are either fewer protons in the vicinity of ^{31}P or increased mobility either from the acid site moieties or from the TMPO molecules. Interestingly, slight shift towards higher ppm (64 ppm) is observed for the Nb_2O_5-B-300 indicating the presence of stronger Brønsted acid sites with respect to those observed in the case of Nb_2O_5-B sample [47]. Furthermore, one can clearly observe the reduction of the relative intensity of the resonance at 64 ppm after the calcination at 500 °C indicating the overall decrease in acid sites amount (see Table 3). These results are in accordance with the results obtained by NH_3-TPD reported in Fig. 8 and Table 2. Whereas the Nb_2O_5-B-300 compared to the as-synthesized sample exhibited similar ratio at 62 ppm proving that the thermal treatment at 300 °C does not affect the amount of acid sites. Combining ssNMR and ICP techniques

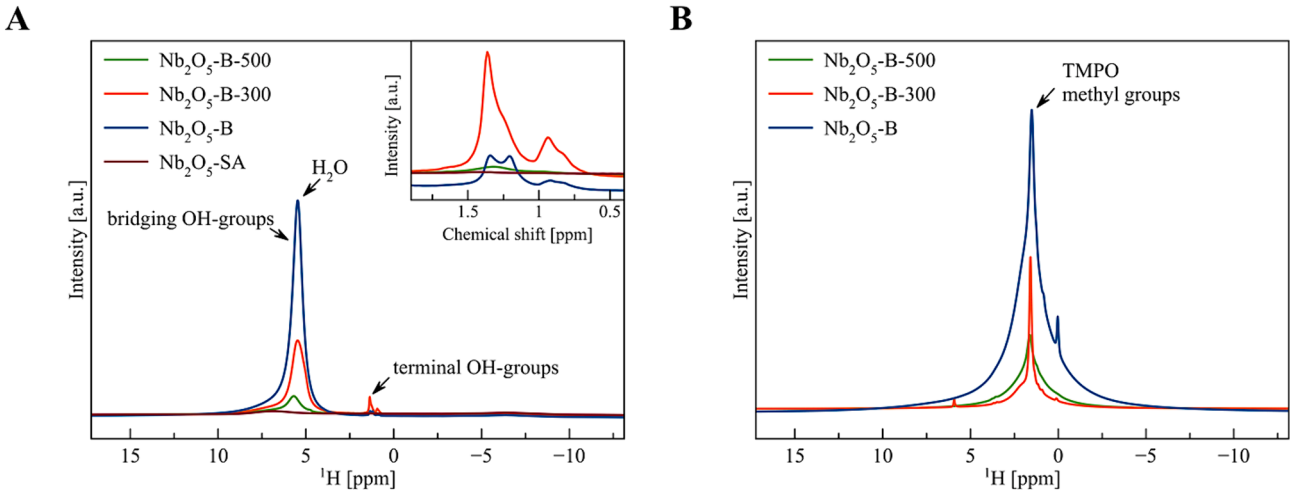

Fig. 9. ^1H MAS NMR spectra of bare niobium oxide samples non-calcined and calcined at different temperatures with the 0.4–1.9 ppm magnified range on the Inset (A) and loaded with 1.4–2.1 mmol (TMPO)/g_{sample} (B) recorded at 700 and 400 MHz using a MAS rate of 40 and 15 kHz, respectively. In panel (A) the spectrum of Nb_2O_5-SA sample is also reported for the sake of comparison.

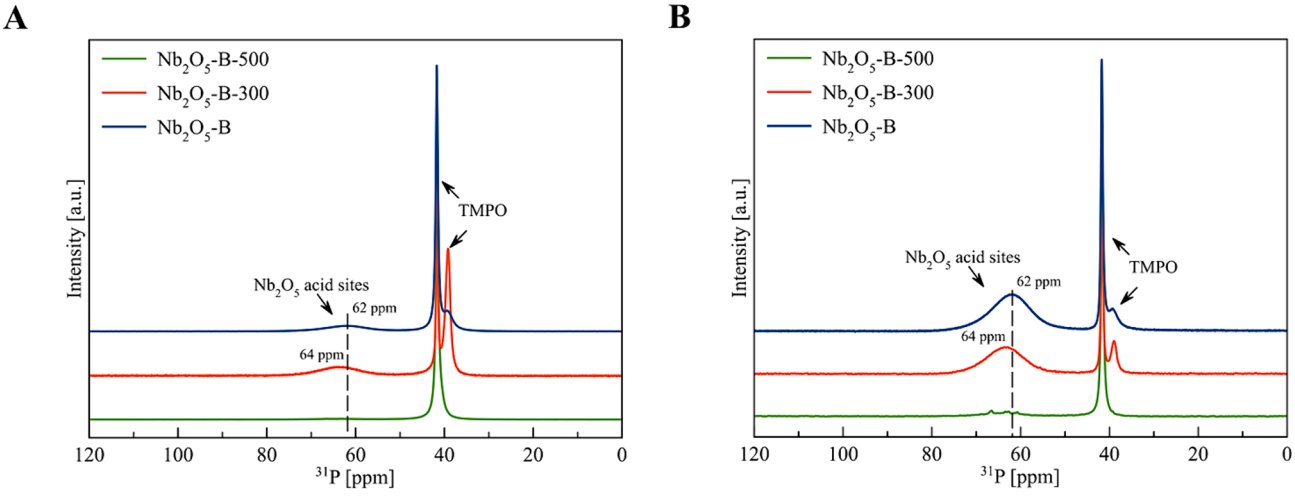

Fig. 10. ^1H-decoupled ^{31}P MAS (A) and ^{31}P CPMAS (B) NMR spectra of niobium oxide samples non-calcined and calcined at different temperatures loaded with 1.4–2.1 mmol (TMPO)/g_{sample} recorded at 400 MHz using a MAS rate of 15 kHz.

Table 3
Relative intensities (%) obtained from the deconvolution of the ^{1}H-decoupled ^{31}P MAS spectra (Fig. 11) of the Nb_2O_5 samples loaded with TMPO and the total amount of acid sites.

Sample	^{31}P resonances [ppm]	Relative intensity (%)	Total acid sites by TMPO [mmol TMPO·g^{-1}]
Nb_2O_5-B	62	23.1	0.48
	42	58.7	
	39	18.2	
Nb_2O_5-B-300	62	26.5	0.42
	42	25.3	
	39	48.2	
Nb_2O_5-B-500	62	3.2	0.05
	42	80.3	
	39	16.5	

(ICP results are presented in Table 4, spectra deconvolution is shown in Fig. 11) it is possible to quantify the concentration of acid sites in solids. Table 3 reports the obtained results, which are comparable with those obtained by means of NH_3-TPD and NaOH titration (Table 2) as well as with those presented earlier in literature [33].

^{1}H–^{31}P 2D HETCOR experiments (Fig. 12) were conducted to elucidate the nature of the acid sites, i.e., Brønsted vs Lewis, observed upon TMPO adsorption. All ^{31}P resonances exhibit a correlation peak with ^{1}H resonances ranging from 0 to 2 ppm, assigned to the autocorrelation with the methyl groups of TMPO. The correlation of the peak at 62 ppm on ^{31}P spectra with a ^{1}H resonance at 14.5 ppm was found only for the Nb_2O_5-B sample (Fig. 12(A)). Usually, ^{1}H resonances higher than 10 ppm indicate the presence of protonated $TMPOH^{+}$ species, H-bonded to the conjugate base of a Brønsted acid site [48]. In the case of Nb_2O_5-B-300 (Fig. 12(B)), the reason explaining the absence of this correlation is most likely the conversion of Brønsted acid sites to Lewis ones due to the partial oxide dehydration during the thermal treatment. While the interaction with a Brønsted acid site is H-mediated, the interaction with a Lewis acid site occurs by the direct interaction between TMPO and an Nb site, thus not resulting in a high ^{1}H chemical shifts correlation typical of H-bonded species. For the Nb_2O_5-B-500 the significant reduction of the peak area at around 62–64 ppm was observed suggesting the reduced amount of total acid sites in this sample comparing to Nb_2O_5-B-300 and Nb_2O_5-B. Moreover, the correlation with ^{1}H signals at high chemical shift values was not detectable, as shown in Fig. 12 (C), thus, it gives us grounds to suggest that the overall acidity of this material is due to the presence of Lewis acid sites. The rational behind the acid sites being converted to Lewis upon sample temperature treatment is also supported elsewhere [49], where a resonance near 62 ppm observed on the ^{31}P spectra of TMPO-loaded zeolite was ascribed to external Lewis acid sites.

While the overall amount of the acid sites in Nb_2O_5-B and Nb_2O_5-B-300 measured from the integration of the ^{31}P peak at around 62–64 ppm is comparable (Table 3), the ^{1}H-^{31}P HETCOR spectra suggest a distinct nature of acid sites, i.e., Brønsted vs Lewis. This fact, as we will discuss in the next section concerning the catalytic activity of the samples, indicates that the presence of Lewis acid sites plays a crucial role in the glucose conversion to 5-HMF.

3.2. Heterogeneous catalytic activity: Glucose valorisation

Preliminary runs towards the optimization of experimental conditions revealed that the best glucose to 5-HMF conversion is reached when the reaction is carried out at 180 °C for 1 h in the presence of 24 mL of 2.3 mM glucose aqueous solution containing 1 g L^{-1} of Nb_2O_5 catalyst. Table 5 compiles the glucose conversion, the selectivity to fructose and to 5-HMF and yield of 5-HMF in the presence of various catalysts.

Table 4
Results of elemental analysis by ICP-OES (in mass %).

Sample	Nb [%]	P [%]
Nb_2O_5-B	46	6.4
Nb_2O_5-B-300	54	4.9
Nb_2O_5-B-500	57	4.4

A perusal of the results reported in Table 5 evidenced that the highest conversion of glucose was obtained in the presence of Nb_2O_5-B, whereas Nb_2O_5-B-300 was the catalyst exhibiting the highest reaction selectivity and yield to 5-HMF. It is worth noting that these two materials are among those exhibiting the strongest acidity (see NH_3-TPD, titration and NMR studies) and the higher SSA. Moreover, the presence of Lewis acid sites in the Nb_2O_5-B-300 sample (as evidenced by the NMR study), favoring the isomerization of glucose into fructose, could be the reason for the larger selectivity, to 5-HMF formation, observed in the presence of this material. The higher content of Lewis acidity in Nb_2O_5-B-300 also explains its increased 5-HMF yields over Nb_2O_5-B-500. A further catalytic run, in the presence of Nb_2O_5-B-300, was performed by using a glucose aqueous solution containing ca. 270 ppm of chloride ions (from ammonium chloride) that simulate the salt content of the algae dispersion. The presence of chlorides decreased the glucose conversion, albeit the selectivity to 5-HMF remained almost constant, hence decreasing the glucose to 5-HMF reaction yield. It is interesting to note that at the same time, the selectivity to fructose increased from 4 to 18 %. These results suggest that the presence of chloride ions not only reduce glucose conversion, but it also inhibits the formation of by-products other than fructose and 5-HMF which, however, have not been detected by HPLC.

3.3. *Chlorella* sp. Valorisation

3.3.1. Carbohydrate content of the *Chlorella* sp.

The carbohydrate content in the algae was estimated with the methodology described in the NREL protocol [34]. The percentage of the sugars content in the lyophilized algae biomass measured by the NREL procedure was 12 %. Consequently, in order to determine the yield towards the furan products obtained in all the hydrothermal reactions reported in this work for the *Chlorella* sp. valorisation (see equation (5), this figure was considered as the maximum amount of sugars derived from the biomass.

3.3.2. Homogeneous and heterogeneous catalytic valorisation of the carbohydrate content of *Chlorella* sp.

The microalgae biomass was catalytically treated under hydrothermal conditions in both homogeneous and heterogeneous regimes. The results were compared by considering the yield towards furans by equation (5). As already discussed in the introduction section, algae upgrading is much more complex than the glucose transformation to 5-HMF, because it requires a first cell membrane degradative step to convert the microalgal biomass, in which the carbohydrates are released in solution. Further steps are the hydrolysis of the polysaccharides to hexoses, essentially glucose, and, hence, its isomerization to fructose on Lewis acid sites followed by dehydration to 5-HMF over Brønsted acid sites. The results of preliminary experiments, carried out with 40 mg of lyophilized *Chlorella* sp. in 24 mL of aqueous suspension, are reported in

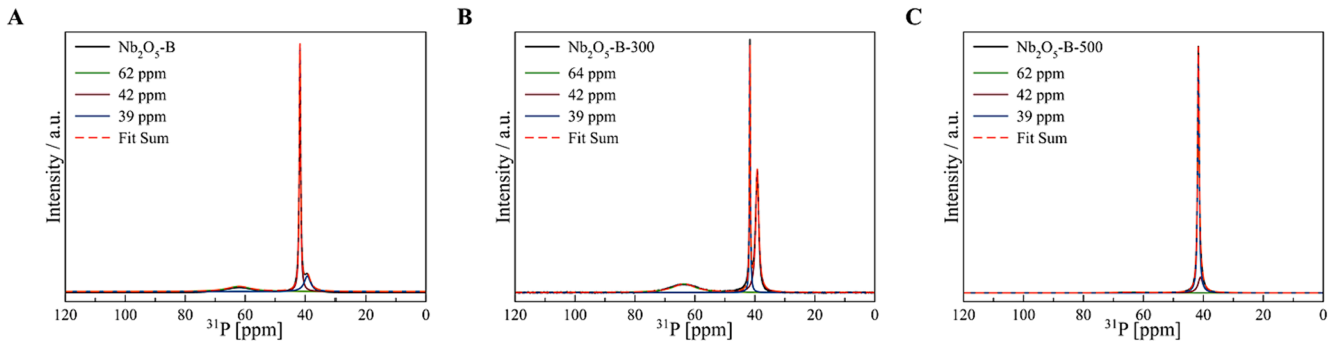

Fig. 11. Deconvolution of the ^{1}H-decoupled ^{31}P MAS NMR spectra of niobium oxide samples calcined at different temperatures loaded with 1.4–2.1 mmol (TMPO)/g_{sample} recorded at 400 MHz using a MAS rate of 15 kHz.

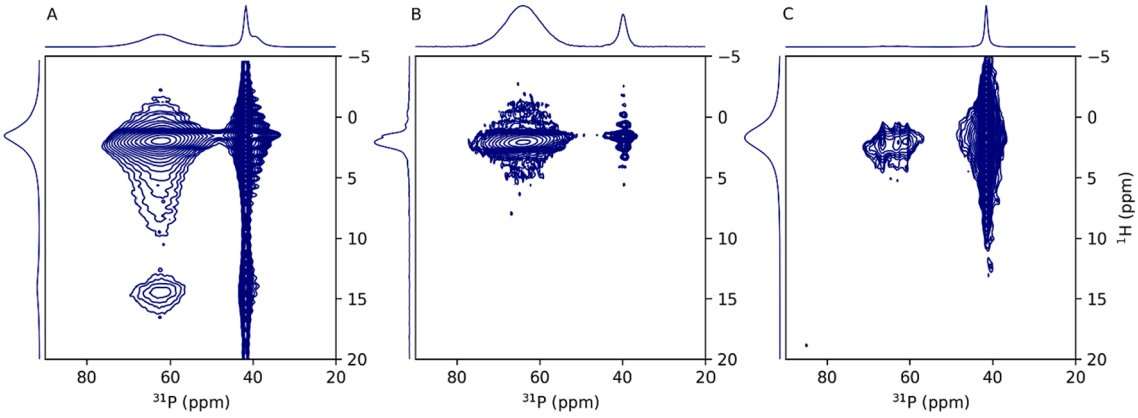

Fig. 12. Two-dimensional (2D) ^{1}H-^{31}P heteronuclear correlation (HETCOR) NMR spectra of Nb_2O_5 samples loaded with 1.4–2.1 mmol (TMPO)/g (sample). A) Nb_2O_5-B; (B) Nb_2O_5-B-300 and (C) Nb_2O_5-B-500.

Table 5
Glucose conversion (X), selectivity to fructose and 5-HMF and yield to 5-HMF, after 1 h of reaction at 180 °C.

Catalyst	X [%]	$S_{fructose}$ [%]	$S_{5\text{-HMF}}$ [%]	$Y_{5\text{-HMF}}$ [%]
Nb_2O_5-T	67	29	30	20
Nb_2O_5-E	65	12	32	21
Nb_2O_5-B	98	1	30	29
Nb_2O_5-B-300	91	4	36	33
Nb_2O_5-B-500	59	7	19	11
Nb_2O_5-SA	44	24	21	9
HY-340	47	22	21	10
Nb_2O_5-B-300[a]	75	18	35	26

[a] Experiment carried out in the presence of 270 ppm of chloride anions.

Table 6 in terms of yield of furans (5-HMF as majority and furfural as minority observed species). In the absence of catalyst at 120 °C for 6 h, no formation of furans was observed (Table 6, entry 1). Conversely, the presence of HCl (homogeneous catalyst) at 140–160 °C and different reaction times, gave rise to modest yields in furans (Table 6, entries 2–6). Due to the low algae conversion, probably due to the difficulty to release sugars in solution, further experiments were performed by adding SiO_2 beads to the suspension to increase the mechanical damage of the cells with the expectation of favouring this preliminary step. Unfortunately, in any case, the yield to furans were still very low (Table 6, entries 7–12). Finally, the heterogeneous conversion of *Chlorella* sp. was performed in the presence of the Nb_2O_5-T catalyst, both in the absence and in the presence of the SiO_2 beads (Table 6, entries 13 to 21). The presence of only Nb_2O_5-T at 120 °C for 2 or 4 h gave negligible yields of the products, probably due to the lack of release of sugars from the biomass. The additional presence of SiO_2 pellets, together with the Nb_2O_5 catalyst, did not change the yield in furans. In any case, the yields were still very low even for long reaction times. It is likely that the difficult release of sugars in solution, as indirectly confirmed by some tests (Table 6, entries 18–21) at different temperatures, could be the cause of the low yields of furans.

The results reported in Table 6 indicate that in order to transform the carbohydrates contained in the algal biomass into furans, the process needs two different steps. The first one aimed at the release and hydrolysis of carbohydrates from the algae to give sugars (essentially glucose) and the second relates to the catalytic conversion of sugars into furans. The first step was then carried out by treating the aqueous suspension of *Chlorella* sp. for 2 h at 140 °C in the presence of SiO_2 beads. After the filtration, the solution underwent a second treatment, at 180 °C for 1 h, in the presence of the various Nb_2O_5 catalysts. The obtained yields in furans (Fig. 13(A)), were still very low though. Consequently, an optimization of both stages was performed. The first step gave the maximum release of carbohydrates from the algae at 180 °C for 2 h in the presence of acetic acid (pH = 4) and of SiO_2 beads. The optimization of the second step was performed at 180 °C in the presence of Nb_2O_5-T by changing the reaction time. As shown in Fig. 13(B), the maximum yield to furans was reached after 10 h of reaction, while for longer reaction times it decreased, probably due to polymerization reactions (see Scheme 1). It is important to underline that in order to test the stability of the catalyst, after the run conducted for 16 h (Fig. 13(B)), the Nb_2O_5-T powder was washed three times with hot water in order to clean its surface. Then a second run of 10 h was carried out and subsequently the catalyst was washed again and a third test of 10 h was performed with the same Nb_2O_5-T powder. These tests showed an excellent stability of the material, which at the third cycle showed a lowering of the maximum furans yield of approximately 8 %, probably due to the loss of

Table 6
Total yield (Y_F) to 5-HMF and furfural from sugars contained in algae for experiments carried out with *Chlorella sp*. under different experimental conditions.

	ID	SiO_2	Reaction time [h]	Temperature [°C]	HCl [% wt]	Amount of Nb_2O_5 [$g_{catalyst}/g_{biomass}$]	Y_F [%]
Homogeneous	1	–	6	120	–	–	0.0
	2	–	2	140	7	–	7
	3	–	3	140	7	–	6
	4	–	6	140	7	–	10
	5	–	16	140	7	–	4
	6	–	2	160	7	–	6
Presence of SiO_2 pellets	7	Yes	6	120	–	–	0.0
	8	Yes	0.33	120	2	–	9
	9	Yes	2	120	2	–	6
	10	Yes	4	120	2	–	8
	11	Yes	6	120	2	–	8
	12	Yes	2	120	0.7	–	7
Heterogeneous (Nb_2O_5-T)	13	–	2	120	–	0.6	0.1
	14	–	4	120	–	0.6	0.1
	15	Yes	2	120	–	0.6	0.1
	16	Yes	4	120	–	0.6	0.1
	17	Yes	23	120	–	0.6	0.2
	18	Yes	6	120	–	0.6	0.0
	19	Yes	6	140	–	0.6	0.0
	20	Yes	6	160	–	0.6	0.1
	21	Yes	6	180	–	0.6	0.2

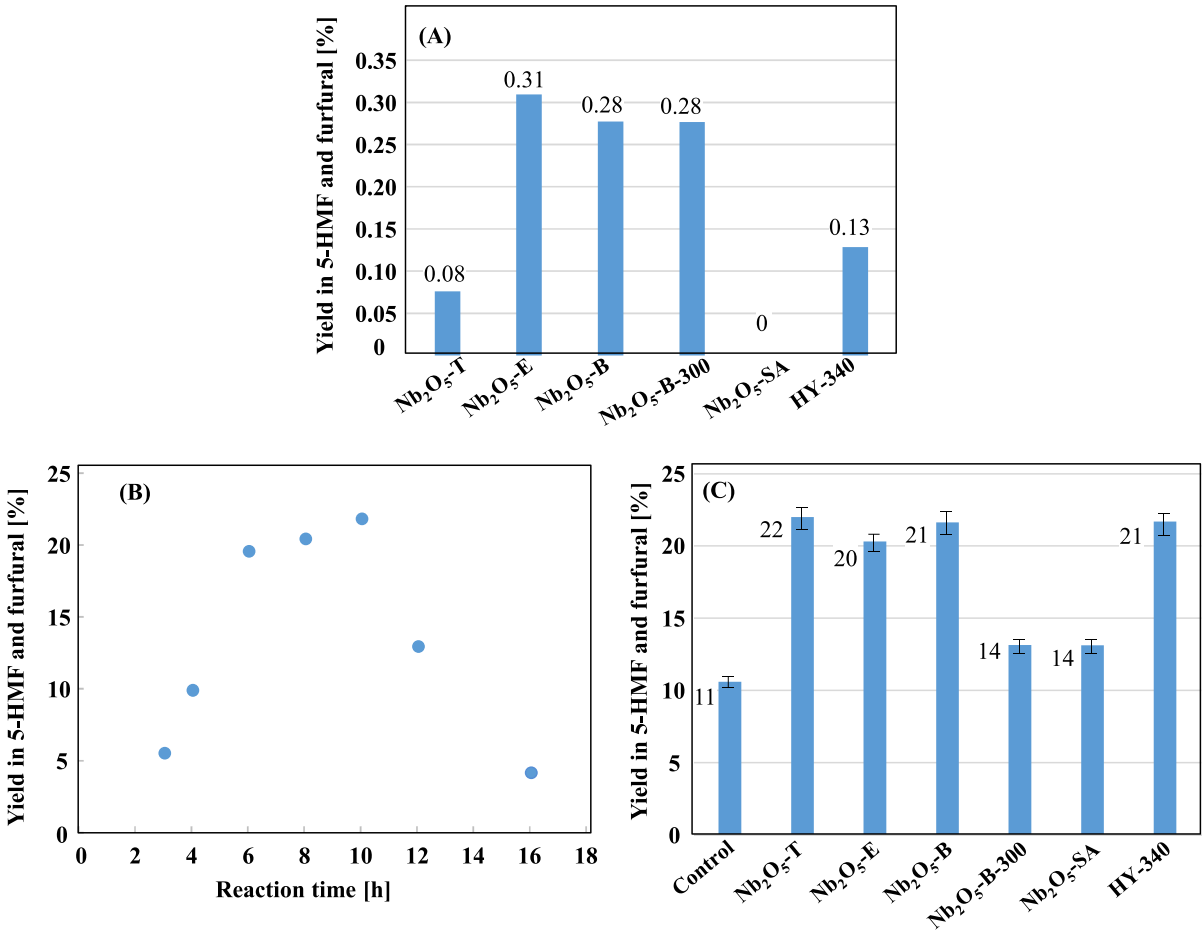

Fig. 13. Total yield to 5-HMF and furfural for runs carried out in two stages (A) the first one in the presence of only SiO_2 (2 h at 140 °C), and the second in the presence of Nb_2O_5 (1 h at 180 °C); (B) the first one in the presence of acetic acid (pH = 4) and SiO_2 (2 h at 180 °C), and the second in the presence of Nb_2O_5-T at 180 °C by varying the reaction time; and (C) the first one as in (B) but the second stage was carried out in the absence (control test) or in the presence of the various Nb_2O_5 materials at 180 °C for 10 h.

small quantities of catalyst that inevitably occurs during the washing process.

After the optimization of the second step, performed in the presence of Nb_2O_5-T, also the activity of the other catalysts was tested under the same condition (Fig. 13(C)). Only the Nb_2O_5-B-500 sample, was not tested because compared to the other Nb_2O_5-B samples, it resulted in

much lower activity in the glucose conversion tests to 5-HMF (see Table 5) in agreement also with ref. [50]. The catalyst recycling tests were performed also in the presence of the other catalysts and in Fig. 13 (C) the oscillation of the result obtained is shown for each material.

For all runs, the quantity of *Chlorella* sp. was 40 mg in 24 mL of water. The amounts of Nb_2O_5 and SiO_2 beads were 24 mg and 240 mg, respectively. The perusal of Fig. 13(C) indicates that Nb_2O_5-T, -E, -B and HY-340 show similar performances in terms of furans yields (essentially 5-HMF), whereas Nb_2O_5-B-300 and Nb_2O_5-SA exhibited lower activities. These results can be attributed to the higher acidity exhibited by the non-calcined solids with respect to the calcined ones including Nb_2O_5-SA that showed moreover a very low specific surface area.

Comparing the results in terms of 5-HMF yield, obtained from the synthetic glucose solution with those achieved starting from *Chlorella* sp. algae, it appears evident that in some cases the total performance of the catalysts dramatically changes. For instance, Nb_2O_5-B-300 exhibited the highest yield to furans from glucose and conversely one of the lowest values of yield from *Chlorella* sp. On the other hand, the HY-340 showed an opposite behavior. It is possible to observe that the best catalysts for the *Chlorella* sp. valorization to furans are those presenting the highest number of Brønsted acid sites. On the contrary, for the conversion of glucose to 5-HMF, the presence of both Lewis and Brønsted sites in the catalyst seems to be essential. Indeed, Lewis acid sites are fundamental for the isomerization of glucose to fructose and Brønsted sites are needed for the dehydration of the latter into 5-HMF. The acid properties studied by ssNMR indicates that Nb_2O_5-B-300 is the sample with the greatest amount of Lewis sites, therefore, justifying the higher yield of 5-HMF starting from a glucose solution. Instead, when *Chlorella* sp. water suspension was the starting material after the first stage (dedicated to the release of carbohydrates present in the algae and their hydrolysis), part of them remained in the form of polysaccharides whose hydrolysis to hexoses and pentoses is favored by the presence of Brønsted acids. Consequently, the most acidic catalysts are those capable to better hydrolyze the residual polysaccharides to monosaccharides that can be transformed to furans with the highest yield.

4. Conclusions

A set of home prepared and commercial Nb_2O_5 catalysts were used for the valorisation of carbohydrates contained in the microalga *Chlorella* sp. to obtain added value products as 5-HMF and furfural. Glucose served as model substrate to study the behaviour of the different Nb_2O_5 materials and optimise the reaction conditions for its conversion to fructose and subsequently to 5-HMF. Preliminary tests were carried out on *Chlorella* sp. under homogeneous or heterogeneous conditions, yielding low furan yields. These low yields were attributed to the complex structure of the cell wall. To optimize the valorization process of microalga *Chlorella* sp. into furans, a two-step reaction was employed, in which the first step facilitated not only the release of carbohydrates into the aqueous solution but also their partial hydrolysis to hexoses and pentoses. This first step was followed by the heterogeneous catalytic reaction in the presence of Nb_2O_5, obtaining a significant increase of the yield to furans up to the 22 % with respect to the total sugars extracted from algae. The employed catalysts were thoroughly characterized by employing various techniques. The findings revealed a clear correlation between conversion yields to 5-HMF and furfural and catalyst acidity, specific surface area, and the existence of Lewis and Brønsted acid sites. While Nb_2O_5-B-300, the catalyst presenting the highest amount of Lewis acid sites, proved to be the best material for glucose transformation into 5-HMF, the catalysts showing the highest number of Brønsted acid sites appeared to be the best ones for the transformation of the complex substrate *Chlorella* sp. Therefore, this study demonstrates the feasibility of the process of conversion into furans of *Chlorella* sp. in the presence of Nb_2O_5, an eco-friendly catalyst, along with an indication on the choice of the optimal catalyst when working with complex matrices substrates.

CRediT authorship contribution statement

Serena Lima: Conceptualization, Data curation, Formal analysis, Investigation, Methodology, Writing – original draft, Writing – review & editing, Supervision. **Elisa I. García-López:** Conceptualization, Investigation, Methodology, Supervision, Writing – original draft, Writing – review & editing. **Igor Krivtsov:** Investigation, Writing – original draft. **Marina Ilkaeva:** Conceptualization, Data curation, Investigation, Writing – review & editing. **Carlos Bornes:** Data curation, Investigation. **Luís Mafra:** Data curation, Funding acquisition, Writing – original draft. **Leonarda F. Liotta:** Data curation, Formal analysis, Investigation, Writing – original draft, Writing – review & editing. **Silvia Villar-Rodil:** Investigation, Writing – original draft. **Juan I. Paredes:** Investigation, Writing – original draft. **Giuseppe Marcì:** Conceptualization, Data curation, Formal analysis, Investigation, Supervision, Writing – original draft, Writing – review & editing, Project administration. **Francesca Scargiali:** Data curation, Funding acquisition, Supervision, Writing – original draft.

Declaration of competing interest

The authors declare that they have no known competing financial interests or personal relationships that could have appeared to influence the work reported in this paper.

Data availability

Data will be made available on request.

Acknowledgements

IK acknowledges support by Spanish MCINN (PID2020-113558RB-C41) and Gobierno del Principado de Asturias (IDI-2021-000048). SV-R and JIP gratefully acknowledge funding by Spanish Ministerio de Ciencia e Innovación and Agencia Estatal de Investigación (MCIN/AEI/10.13039/501100011033) as well as the European Regional Development Fund (ERDF, A way of making Europe) through grant PID2021-125246OB-I00, and by Plan de Ciencia, Tecnología e Innovación (PCTI) 2018-2022 del Principado de Asturias and by ERDF through grant IDI/2021/000037. This work was developed within the scope of the project CICECO-Aveiro Institute of Materials, UIDB/50011/2020, UIDP/50011/2020, and LA/P/0006/2020, financed by national funds through the FCT/MEC (PIDDAC). We also acknowledge funding from project PTDC/QUI-QFI/28747/2017 (GAS2MAT-DNPSENS-POCI-01-0145-FEDER-028), financed through FCT/MEC and cofinanced by FEDER under the PT2020 Partnership Agreement. The NMR spectrometers are part of the National NMR Network (PTNMR) and are partially supported by Infrastructure Project 022161 (cofinanced by FEDER through COMPETE 2020, POCI and PORL, and FCT through PIDDAC). SL acknowledges support by European Research Council (ERC) under the European Union's Horizon 2020 research and innovation program (Grant Agreement 865974) and with the co-funding of European Union, European Social Fund – REACT EU, PON Ricerca e Innovazione 2014-2020, Azione IV.4 "Dottorati e contratti di ricerca su tematiche dell'innovazione" and Azione IV.6 "Contratti di ricerca su tematiche Green" (DM 1062/2021). MI acknowledges FCT for Researcher Position (CEECIND/00546/2018) and Beatriz Galindo Scholarship (MU-23-BG22/00145).

References

[1] J. Goldemberg, Ethanol for a sustainable energy future, Science 315 (2007) 808–810.
[2] C.O. Tuck, E. Pérez, I.T. Horváth, R.A. Sheldon, M. Poliakoff, Valorization of biomass: deriving more value from waste, Science 337 (2012) 695–699.

[3] A.C. Guedes, H.M. Amaro, F.X. Malcata, Microalgae as sources of high added-value compounds—a brief review of recent work, Biotechnol. Progress 27 (2011) 597–613.

[4] H. Xu, X. Li, W. Hu, L. Lu, J. Chen, Y. Zhu, H. Zhou, C. Si, Recent advances on solid acid catalyic systems for production of 5-hydroxymethylfurfural from biomass derivatives, Fuel Process. Technol. 234 (2022) 107338.

[5] T. Wang, M.W. Nolte, B.H. Shanks, Catalytic dehydration of C6 carbohydrates for the production of hydroxymethylfurfural (HMF) as a versatile platform chemical, Green Chem. 16 (2014) 548–572.

[6] S.P. Teong, G. Yi, Y. Zhang, Hydroxymethylfurfural production from bioresources: past, present and future, Green Chem. 16 (2014) 2015–2026.

[7] A. Marshall, B. Jiang, R.M. Gauvin, C.M. Thomas, 2,5-furandicarboxylic acid: an intriguing precursor for monomer and polymer synthesis, Molecules 27 (2022) 4071.

[8] R. Mariscal, P. Maireles-Torres, M. Ojeda, I. Sádaba, M. López Granados, Furfural: a renewable and versatile platform molecule for the synthesis of chemicals and fuels, Energy Environ. Sci. 9 (2016) 1144–1189.

[9] S. Zhong, R. Daniel, H. Xu, J. Zhang, D. Turner, M.L. Wyszynski, P. Richards, Combustion and emissions of 2,5-dimethylfuran in a direct-injection spark-ignition engine, Energy Fuels 24 (5) (2010) 2891–2899.

[10] J. Lewkowski, Synthesis, chemistry and applications of 5-hydroxymethyl-furfural and its derivatives, Arkivoc. 2001 (2001) 17–54.

[11] X. Tong, Y. Ma, Y. Li, Biomass into chemicals: conversion of sugars to furan derivatives by catalytic processes, Appl. Catal. A Gen. 385 (2010) 1–13.

[12] L.T. Mika, E. Cséfalvay, Á. Németh, Catalytic conversion of carbohydrates to initial platform chemicals: chemistry and sustainability, Chem. Rev. 118 (2018) 505–613.

[13] R.J. Van Putten, J.C. Van Der Waal, E. De Jong, C.B. Rasrendra, H.J. Heeres, J. G. De Vries, Hydroxymethylfurfural, a versatile platform chemical made from renewable resources, Chem. Rev. 113 (2013) 1499–1597.

[14] V. Choudhary, S.H. Mushrif, C. Ho, A. Anderko, V. Nikolakis, N.S. Marinkovic, A. I. Frenkel, S.I. Sandler, D.G. Vlachos, Insights into the interplay of Lewis and brønsted acid catalysts in glucose and fructose conversion to 5-(hydroxymethyl) furfural and levulinic acid in aqueous media, J. Am. Chem. Soc. 135 (2013) 3997–4006.

[15] B. Agarwal, K. Kailasam, R.S. Sangwan, S. Elumalai, Traversing the history of solid catalysts for heterogeneous synthesis of 5-hydroxymethylfurfural from carbohydrate sugars: a review, Renewable and Sustainable Energy Reviews 82 (2018) 2408–2425.

[16] J. Esteban, A.J. Vorholt, W. Leitner, An overview of the biphasic dehydration of sugars to 5-hydroxymethylfurfural and furfural: a rational selection of solvents using COSMO-RS and selection guides, Green Chem. 22 (2020) 2097–2128.

[17] I.K.M. Yu, D.C.W. Tsang, Conversion of biomass to hydroxymethylfurfural: a review of catalytic systems and underlying mechanisms, Biores. Tech. 238 (2017) 716–732.

[18] K. Nakajima, J. Hirata, M. Kim, N.K. Gupta, T. Murayama, A. Yoshida, N. Hiyoshi, A. Fukuoka, W. Ueda, Facile formation of lactic acid from a triose sugar in water over niobium oxide with a deformed orthorhombic phase, ACS Catal. 8 (2018) 283–290.

[19] S. Sumiya, Y. Oumi, M. Sadakane, T. Sano, Facile preparation of SBA-15-supported niobic acid (Nb2O5·nH2O) catalyst and its catalytic activity, App. Catal A 365 (2009) 261–267.

[20] I. Nowak, M. Ziolek, Niobium compounds: preparation, characterization, and application in heterogeneous catalysis, Chem. Rev. 99 (1999) 3603–3624.

[21] K. Tanabe, S. Okazaki, Various reactions catalyzed by niobium compounds and materials, App. Catal. A 133 (1995) 191–218.

[22] S. Lima, A. Brucato, G. Caputo, F. Grisafi, F. Scargiali, Inoculum of indigenous microalgae/activated sludge for optimal treatment of municipal wastewaters and biochemical composition of residual biomass for potential applications, J. Water Process Eng. 103142 (2022).

[23] S. Lima, J. Lokesh, P.S.C. Schulze, R.H. Wijffels, V. Kiron, F. Scargiali, S. Petters, H. C. Bernstein, D. Morales-Sánchez, Flashing lights affect the photophysiology and expression of carotenoid and lipid synthesis genes in nannochloropsis gaditana, J. of Biotech. 360 (August) (2022) 171–181.

[24] V. Villanova, C. Galasso, F. Fiorini, S. Lima, M. Brönstrup, C. Sansone, C. Brunet, A. Brucato, F. Scargiali, Biological and chemical characterization of new isolated halophilic microorganisms from saltern ponds of Trapani, Sicily, Algal Res. 54 (2021) 102192.

[25] S. Lima, E.I. García-López, A. Adawy, G. Marcì, F. Scargiali, Valorisation of chlorella sp. biomass in 5-HMF through a two-step conversion in the presence of Nb2O5 and NbOPO4 and optimisation through reactive extraction, Chem. Eng. J. 471 (2023) 144583.

[26] J.J. Wang, Z.C. Tan, C.C. Zhu, G. Miao, L.Z. Kong, Y.H. Sun, One-pot catalytic conversion of microalgae (chlorococcum sp.) into 5-hydroxymethylfurfural over the commercial H-ZSM-5 zeolite, Green Chem. 18 (2016) 452–460.

[27] M.L. Testa, V. La Parola, L.F. Liotta, A.M. Venezia, Screening of different solid acid catalysts for glycerol acetylation, J. Mol. Catal. A 367 (2013) 69–76.

[28] Y. Narendar, G.L. Messing, Synthesis, decomposition and crystallization characteristics of Peroxo−Citrato−Niobium: an aqueous niobium precursor, Chem. Mater. 9 (1997) 580–587.

[29] C. Tagusagawa, A. Takagaki, S. Hayashi, K. Domen, Evaluation of strong acid properties of layered $HNbMoO_6$ and catalytic activity for friedel-crafts alkylation, Catal. Today 142 (2009) 267–271.

[30] C. Tagusagawa, A. Takagaki, A. Iguchi, K. Takanabe, J.N. Kondo, K. Ebitani, S. Hayashi, T. Tatsumi, K. Domen, Highly active mesoporous Nb-W oxide solid-acid catalyst, Angew. Chemie - Int. Ed. 49 (2010) 1128–1132.

[31] K. Nakajima, Y. Baba, R. Noma, M. Kitano, J.N. Kondo, S. Hayashi, M. Hara, $Nb_2O_5{\cdot}nH_2O$ as a heterogeneous catalyst with water-tolerant Lewis acid sites, J. Am. Chem. Soc. 133 (2011) 4224–4227.

[32] H.T. Kreissl, M.M.J. Li, Y.K. Peng, K. Nakagawa, T.J.N. Hooper, J.V. Hanna, A. Shepherd, T.S. Wu, Y.L. Soo, S.C.E. Tsang, Structural studies of bulk to nanosize niobium oxides with correlation to their acidity, J. Am. Chem. Soc. 139 (2017) 12670–12680.

[33] H.T. Kreissl, K. Nakagawa, Y.K. Peng, Y. Koito, J.L. Zheng, S.C.E. Tsang, Niobium oxides: correlation of acidity with structure and catalytic performance in sucrose conversion to 5-hydroxymethylfurfural, J. Catal. 338 (2016) 329–339.

[34] S. Van Wychen, L.M.L. Laurens, Determination of total carbohydrates in algal biomass - laboratory analytical procedure (LAP), Lab. Anal. Proced. 18 (2015). www.nrel.gov/publications.

[35] M. Thommes, K. Kaneko, A. V. Neimark, J. P. Olivier, F. Rodriguez-Reinoso, J. Rouquerol K. S.W. Sing, Pure Appl. Chem. IUPAC Technical Report. 2015, http://sol.rutgers.edu/~aneimark/PDFs/IUPAC_Report_PAC_2015.pdf.

[36] O.F. Lopes, E.C. Paris, C. Ribeiro, Synthesis of Nb_2O_5 nanoparticles through the oxidant peroxide method applied to organic pollutant photodegradation: a mechanistic study, App. Catal. B 144 (2014) 800–808.

[37] J.M. Jehng, I.E. Wachs, Structural chemistry and raman spectra of niobium oxides, Chem. Mater. 3 (1991) 100–107.

[38] K. Yoshimura, T. Miki, S. Iwawa, S. Tanemura, Niobium oxide electrochromic thin films prepared by reactive DC magnetron sputtering, Jpn. J. Appl. Phys. 34 (1995) L1293.

[39] T. Ikeya, M. Senna, Change in the structure of niobium pentoxide due to mechanical and thermal treatments, J. Noncryst. Solids 105 (1988) 243–250.

[40] R.M. Pittman, A.T. Bell, Raman studies of the structure of niobium oxide/titanium oxide (Nb2O5/TiO2), J. Phys. Chem. 97 (1993) 12178–12185.

[41] K. Nakamoto, Infrared and raman spectra of inorganic and coordination compounds, 4th edn., Wiley, New York, 1986.

[42] R. Romero, J.R. Ramos-Barrado, F. Martin, D. Leinen, Nb_2O_5 thin films obtained by chemical spray pyrolysis, Surf. Interface Anal. 36 (2004) 888–891.

[43] E.I. García-López, F.R. Pomilla, B. Megna, M.L. Testa, L.F. Liotta, G. Marcì, Catalytic dehydration of fructose to 5-hydroxymethylfurfural in aqueous medium over Nb_2O_5-based catalysts, Nanomaterials 11 (2021) 1821.

[44] I.V. Yakovlev, E. Papulovskiy, E.A. Paukshtis, V.M. Bondareva, A.V. Toktarev, V. I. Zaikovskii, O.B. Lapina, 1H and 93Nb solid-state NMR and IR study of acidity of nanodisperse $Nb_2O_5{\cdot}nH_2O$, Appl. Magn. Reson. 50 (2019) 589–597.

[45] M. Hunger, Multinuclear solid-state NMR studies of acidic and non-acidic hydroxyl protons in zeolites, Solid State Nucl. Magn. Reson. 6 (1996) 1–29.

[46] E.F. Rakiewicz, A.W. Peters, R.F. Wormsbecher, K.J. Sutovich, K.T. Mueller, Characterization of acid sites in zeolitic and other inorganic systems using solid-state ^{31}P NMR of the probe molecule trimethylphosphine oxide, J. Phys. Chem. B 102 (1998) 2890–2896.

[47] A. Zheng, H. Zhang, X. Lu, S.B. Liu, F. Deng, Theoretical predictions of ^{31}P NMR chemical shift threshold of trimethylphosphine oxide absorbed on solid acid catalysts, J. Phys. Chem. B 112 (2008) 4496–4505.

[48] A. Zheng, S.B. Liu, F. Deng, ^{31}P NMR chemical shifts of phosphorus probes as reliable and practical acidity scales for solid and liquid catalysts, Chem. Rev. 117 (2017) 12475–12531.

[49] C. Bornes, D. Stosic, C.F.G.C. Geraldes, S. Mintova, J. Rocha, L. Mafra, Elucidating the nature of the external acid sites of ZSM-5 zeolites using NMR probe molecules, Chem. Eur. J. 28 (2022) e202201795.

[50] K.M. Eblagon, A. Malaika, K. Ptaszynska, M.F.R. Pereira, J.L. Figueiredo, Impact of thermal treatment of Nb_2O_5 on its performance in glucose dehydration to 5-hydroxymethylfurfural in water, Nanomaterials 10 (2020) 1685.